

Research Article

Open Access



Regulatory mechanism of highly transparent, low-thermal-conductivity aerogel film for energy-efficient windows

Nyachieo Kennedy Momanyi^{1,*} , Peng Zhao^{1,*} , Xingyu Liu^{1,*}, Ningfei Sun², Tonghua Hu³, Jianyu Sun¹, Yong Xie^{1,*} , Limin Liu¹

¹School of Physics, Beihang University, Beijing 100191, China.

²Beijing Huairou Laboratory, Beijing 101499, China.

³Hangzhou Institute for Advanced Study, University of Chinese Academy of Sciences, Hangzhou 310024, Zhejiang, China.

*Authors contributed equally to this work and should be considered co-first authors.

*Correspondence to: Dr. Yong Xie, School of Physics, Beihang University, No. 9, South Third Street, Shahe Higher Education Park, Changping District, Beijing 100191, China. E-mail: xiey@buaa.edu.cn

How to cite this article: Momanyi, N. K.; Zhao, P.; Liu, X.; Sun, N.; Hu, T.; Sun, J.; Xie, Y.; Liu, L. Regulatory mechanism of highly transparent, low-thermal-conductivity aerogel film for energy-efficient windows. *Soft Sci.* 2025, 5, 25. <https://dx.doi.org/10.20517/ss.2025.10>

Received: 4 Apr 2025 **First Decision:** 7 May 2025 **Revised:** 14 Jun 2025 **Accepted:** 16 Jun 2025 **Published:** 24 Jun 2025

Academic Editor: YongAn Huang **Copy Editor:** Pei-Yun Wang **Production Editor:** Pei-Yun Wang

Abstract

Aerogels are a focus of research in energy-saving materials due to their unique nanoporous structure. However, achieving aerogels with simultaneously high transparency, low thermal conductivity, and remarkable mechanical robustness remains a challenge. Herein, a highly transparent, low thermal conductivity, and mechanically robust silica aerogel is fabricated through sol-gel process combined with supercritical drying. By systematically optimizing the concentrations of methyltrimethoxysilane, cetyltrimethylammonium bromide, urea, and acetic acid in solution, we obtained an aerogel film with transparency of 97.83 % in the visible spectrum, thermal conductivity of $0.0149 \text{ W}\cdot\text{m}^{-1}\cdot\text{K}^{-1}$, and maximum compressive strain of 27%. When applied as a sandwich material between double glass, it demonstrates significantly enhanced thermal insulation performance while maintaining transparency comparable to that of conventional glass. Furthermore, the silica aerogel film exhibits exceptional hydrophobicity due to the presence of methyl groups, which enhances its structural stability. Consequently, this high-performance silica aerogel film demonstrates strong potential for energy-saving windows, making it an ideal candidate for retrofitting existing buildings and integrating into emerging architectural glazing systems.

Keywords: Silica aerogel film, high transparency, low thermal conductivity, mechanical robustness, energy-saving window



© The Author(s) 2025. **Open Access** This article is licensed under a Creative Commons Attribution 4.0 International License (<https://creativecommons.org/licenses/by/4.0/>), which permits unrestricted use, sharing, adaptation, distribution and reproduction in any medium or format, for any purpose, even commercially, as long as you give appropriate credit to the original author(s) and the source, provide a link to the Creative Commons license, and indicate if changes were made.



INTRODUCTION

Currently, 40%-50% of the global energy production is used for thermal management of buildings^[1,2]. According to the U.S. Department of Energy, about 30% of the energy used to cool and heat buildings is lost through windows due to poor thermal insulation. Consequently, the interior-exterior energy exchange through windows by conduction, convection, and radiation must be minimized to provide favorable indoor conditions, regardless of the outdoor environment, with minimal or no extra energy investment^[3]. However, achieving this through plain monolithic glass, which improves thermal insulation without compromising light transmittance, is challenging^[4].

Thicker glasses, multi-pane glazing filled with air, krypton, argon, or vacuum, and tinting glass panes that absorb solar heat have been developed as energy-efficient window glazing materials. However, thicker glasses characterized by lower U -value, tolerable visible light transmittance, come with high cost and significantly increased overall window weight and volume. Meanwhile, multi-pane glazing is limited in addressing issues related to seal integrity and gas convection^[4,5]. Additionally, tinted glasses trade off transmittance, visibility, and color while absorbing a fraction of solar heat and blocking daylight^[5]. Therefore, there is a need to adopt new materials with low density and low thermal conductivity to curb the energy wastage while maintaining the daylighting requirements of building windows^[6].

Aerogel, a solid material with the lowest density and thermal conductivity^[7-10], has been developed by researchers to improve the energy efficiency of buildings. For example, Abraham *et al.* designed a silanized cellulose aerogel with visible light transmittance of 97% and high hydrophobicity^[4]. Besides, a delaminated aerogel film with high transmittance was fabricated through fluorinated cellulose nanofiber assembly at the solid-liquid interface by Lian *et al.*^[11]. Unfortunately, the commercialization of cellulose aerogel is challenging due to the hindrance of industrial scalability of processes and specialized equipment, as well as slow and tedious preparation methods, moisture sensitivity, and flammability^[12,13]. Furthermore, for long-term exposure, the aging of these organic materials and the stability of their surface also limit their practical performance^[12,14]. In contrast, silica aerogel has advantages in terms of stability, durability, and a relatively simplified preparation process. Therefore, advancing the design and preparation strategy of silica aerogels may be a streamlined approach to realizing commercial energy-saving windows. While prior work has focused on the effects of individual reagents or specific reagent groups on the microstructure of silica aerogels^[15,16], optimizing only a few reagents in a reaction may fail to produce a representative sample, as it overlooks the synergistic roles of all reagents involved.

In this study, we investigated the regulation of silica aerogel microstructure by meticulously and systematically varying all the starting reactants, i.e., concentrations of precursor, solvent, gelation agent, phase separation suppressor, and acid and base catalysts during the sol-gel process. Building upon previous research^[16,17] on the microstructure of aerogel, our comprehensive approach aimed to optimize the pore size to achieve a synergistic balance of high light transmittance, low thermal conductivity, and robust mechanical properties. Finally, an aerogel film with high transparency (97.83% in the visible spectrum) and low thermal conductivity ($0.0149 \text{ W}\cdot\text{m}^{-1}\cdot\text{K}^{-1}$) was achieved. Meanwhile, we proved the feasibility of using it as a sandwich material instead of traditional double glass through control experiments and COMSOL simulations. This optimization is critical for developing highly efficient window materials that meet demanding performance criteria in energy-efficient building applications.

EXPERIMENTAL

Materials

Cetyltrimethylammonium bromide (CTAB, 99%), methyltrimethoxysilane (MTMS, 97%), and urea (99.3%) were purchased from Alfa Aesar. Acetic acid (99%), deionized water (DIW), ethanol (a.r), and isopropanol (a.r) were purchased from Beijing Chemical Plant. All the reagents were used without any further purification. Before the experiment, 200 μ L acetic acid was diluted by 19.8 mL DIW.

Preparation of silica aerogel

The density, specific surface area (SSA), porosity, and mechanical properties of aerogel depend highly on the synthesis conditions and parameters. A high concentration of precursor results in a denser, more interconnected structure, thereby increasing the SSA and porosity. In contrast, a low precursor concentration often leads to structural collapse during solvent exchange and supercritical drying, making it challenging to preserve the aerogel's structure. The choice of solvent is also critical; it must effectively dissolve the precursor to form a homogeneous solution. In this study, DIW was used. An acid catalyzes the hydrolysis step, while urea accelerates the condensation reaction, ultimately influencing the resulting microstructure. In this fabrication process, the CTAB surfactant minimizes phase separation during condensation, contributing to a more uniform structure^[18].

Herein, the acid-base two-step reaction sol-gel method was adopted^[2]. Simply, this method is based on hydrolysis at low temperatures and polycondensation at high temperatures. CTAB and urea were weighed, followed by the addition of DIW, and then subjected to vigorous sonication to form a homogenous solution. Afterward, MTMS and acetic acid were added and then subjected to sonication for 30 min to facilitate the hydrolysis reaction. The content was transferred into a mold and put in DIW in a Petri dish for gel formation and aging at 60 °C in an oven for five days. The ensuing hydrogel was removed from the mold and soaked thoroughly in DIW for 18 h to remove any unreacted reagents. This was followed by sequential solvent exchange in ethanol and isopropanol for 18 h each. Further, CO₂ solvent exchange was carried out for the alcogel formed at 0-10 °C in Samdri-780A, Tousimis critical point drier chamber for eight hours, and ultimately supercritical drying at 37 °C under 8.6 MPa for one hour and then depressurization at 37 °C to form silica aerogel film. It is worth noting that during the solvent exchange process, it is essential to ensure that water and unreacted reagents are gradually replaced by ethanol and isopropyl alcohol. If necessary, a temperature-controlled shaking table can be used for this purpose. During the initial preparation process, the concentration of the parameters was tailored to regulate the network of the aerogel film. The sample codes are defined as M, D, U, C, and A for MTMS (mL), DIW (mL), urea (g), CTAB (g), and diluted acetic acid (μ L), respectively.

Characterization of aerogel film

The morphology of aerogel was characterized by scanning electron microscopy (SEM; SU8000, Hitachi, Japan) after platinum sputtering to enhance electron conductivity. The light transmittance of a 1 cm \times 1 cm \times 0.3 cm film at room temperature characterization was done by ultraviolet-visible (UV-vis) spectroscopy (BX53M, Olympus, JPN). Surface functional groups on the film were characterized by Fourier transform infrared (FTIR) spectroscopy (Nicolet IS10, Thermo Fisher, America). At 77 K, N₂ adsorption-desorption isotherms were measured by v4.0, Quantachrome, America machine. The SSA was determined by the Brunauer-Emmett-Teller (BET) method. At the same time, the pore size and pore size distributions were obtained from the adsorption branch via Barrett-Joyner-Halenda (BJH) calculations. The universal testing machine (Instron E3000K8953) was used to determine the mechanical properties of 1 cm \times 1 cm \times 0.5 cm samples. Thermogravimetric (TG) analysis was conducted by a high-temperature synchronous thermal analyzer (TGA-PT 1600, Linseis, Germany) under N₂ protection to analyze the thermal stability of silica aerogel film. The thermal imager measured the surface temperature of films placed on the desk while the

solar simulator's xenon lamp illuminated the sample with 1 Sun energy density. To investigate the thermal properties, the laser flash transient method, which determines thermal diffusivity (α), was adopted since the pore size of the samples was less than 500 μm ^[19]. The thermal conductivity (λ) was subsequently calculated using

$$\lambda = \alpha \rho c \quad (1)$$

where ρ is the density and c is the specific heat capacity of the aerogel film. Haze meter (TH-110, FIGSPEC, CHN) was used to analyze the light scattering ability of aerogel. Some of the test results and the relationship between density and modulus have been presented in the [Supplementary Materials](#).

Simulation of thermal conductivity

The thermal conductivity was computed by finite element using COMSOL Multiphysics simulation software. Simply, the sandwich structure was designed as shown in the [Supplementary Materials](#) in detail. The upper and lower layers were set as glass with constant thickness (1 mm), and the interlayer as insulation material with adjustable thickness. The specific heat capacity, density, and thermal conductivity values of aerogel, air, polyurethane (PU), and glass were predefined. The two main equations governing the simulation of thermal conductivity are given by

$$\rho C_p \frac{\partial T}{\partial t} + \rho C_p u \cdot \nabla T + \nabla q = Q + Q_{ted} \quad (2)$$

$$q = -k \nabla T \quad (3)$$

where ρ , C_p , T , t , u , Q , Q_{ted} , and k represent the density of the material ($\text{kg} \cdot \text{m}^{-3}$), specific heat capacity at constant pressure ($\text{J} \cdot \text{kg}^{-1} \cdot \text{K}^{-1}$), temperature (K), Time (s), air velocity field ($\text{m} \cdot \text{s}^{-1}$), external heat source term ($\text{W} \cdot \text{m}^{-3}$), thermoelectric heat source ($\text{W} \cdot \text{m}^{-3}$), and thermal conductivity ($\text{W} \cdot \text{m}^{-1} \cdot \text{K}^{-1}$) of material, respectively.

RESULTS AND DISCUSSION

Our design principle begins with the schematic diagrams shown in [Figure 1](#). The acid-base two-step reaction sol-gel method and supercritical drying were employed to prepare the aerogel film, as illustrated in [Figure 1A](#). Transmittance (which refers to the weighted or average transmittance since, in window glazing, overall performance over a range of wavelengths matters) and thermal conductivity are the primary properties to consider for energy-saving materials, and both are closely related to the network structure of aerogel. To achieve this, we optimized the microstructure of the aerogel by tuning the starting compositions to create a mesoscale structure with high light transparency, mechanical robustness, and low thermal conductivity. Each reagent of the starting composition, such as the volume of MTMS, the amount of CTAB, the volume of acetic acid, the volume of solvent, and the amount of urea, was independently varied [[Table 1](#)]. With appropriate concentrations, the aerogel film with high transmittance was obtained.

When light impinges on small particles, it either undergoes Mie scattering or Rayleigh scattering, depending on the particle size. Mie scattering occurs when the particle size is larger than or equal to the wavelength of light, resulting in an increase in haze and a decrease in transmittance [[Figure 1B](#)]. Conversely, for Rayleigh scattering to be dominant, the particle (pore) size should be smaller than the wavelength of visible light, i.e., scattering particle size $< \lambda/10$, where λ is the visible light wavelength^[20]. For instance, Rayleigh scattering dominates in A2 for visible light wavelengths ($\lambda = 400\text{--}700\text{ nm}$) because its pore diameter ($d = 12.6\text{ nm}$) satisfies the condition $d < \lambda/10$ (where $\lambda/10 = 40\text{--}70\text{ nm}$). Generally, Rayleigh scattering explains the haze observed due to small-sized particles in aerogel.

Table 1. Sample code and corresponding chemical dose and transmittance (T)

Sample	CTAB (g)	Urea (g)	DIW (mL)	MTMS (mL)	Acetic acid (μL)	T (%)
M1	0.2	1.5	5	0.5	28.6	70.91
M2	0.2	1.5	5	1	28.6	95.81
M3	0.2	1.5	5	1.5	28.6	89.15
M4	0.2	1.5	5	2	28.6	79.78
U1	0.2	1	5	1	28.6	94.16
U2	0.2	2	5	1	28.6	95.20
U3	0.2	2.5	5	1	28.6	93.62
A1	0.2	1.5	5	1	6	91.93
A2	0.2	1.5	5	1	12	97.83
A3	0.2	1.5	5	1	46	95.23
C1	0.1	1.5	5	1	28.6	87.50
C2	0.3	1.5	5	1	28.6	79.40
C3	0.4	1.5	5	1	28.6	72.70
D1	0.2	1.5	2.5	1	28.6	90.94
D2	0.2	1.5	7.5	1	28.6	84.19
D3	0.2	1.5	10	1	28.6	92.40

The samples with the best transmittance in each group have been highlighted. CTAB: Cetyltrimethylammonium bromide; DIW: deionized water; MTMS: methyltrimethoxysilane.

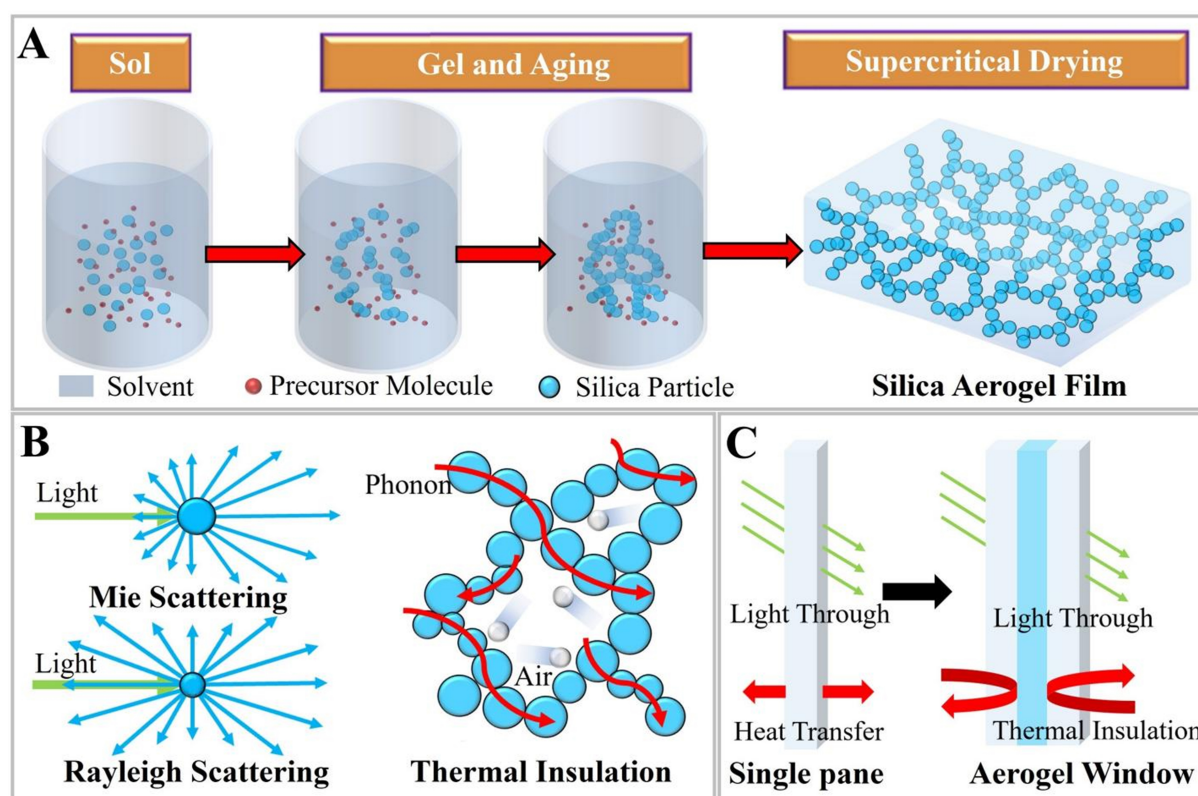


Figure 1. Design philosophy of aerogel window. (A) Microscopic assembly of silica aerogel; (B) Schematic diagrams of the light scattering mechanism and modes of thermal conductivity in aerogel; (C) Schematic diagrams of transmittance and thermal conductivity of a single pane and an aerogel window.

Meanwhile, the optimized network can inhibit phonon heat conduction and gas heat diffusion [Figure 1B]. When silica aerogel exhibits a transmittance comparable to that of glass and has a thermal conductivity lower than that of air, it can be used as a sandwich material to meet the demands of insulation and lighting for windows, once the conditions of mechanical robustness and durability are satisfied [Figure 1C].

To elucidate the transmittance in aerogel further, the particles and the pores act as the nanometric scattering centers, where the intensity (I) of scattered light is given by^[21]

$$I = I_0 \frac{1 + \cos^2 \theta}{2d^2} \left(\frac{2\pi}{\lambda} \right)^4 \left(\frac{n^2 - 1}{n^2 + 2} \right)^2 \left(\frac{r}{2} \right)^6 \quad (4)$$

where r is the pore or particle size, d is the radial distance between the detector and particle, λ is the wavelength of light, n is the refractive index, and θ is the scattering angle. Generally, the scattering intensity is proportional to the sixth power of the pore or particle size, which explains the noticeable discrepancy when the pore or particle sizes slightly vary. Therefore, under the foundational premise of the uniform network, the transmittance of aerogel is enhanced as the pore and particle sizes decrease and vice versa.

The total thermal conductivity (λ) of an aerogel film is the sum of the contributions from solid conduction (λ_s), gas conduction (λ_g), and radiative heat transfer (λ_r). The convoluted pathways and the microstructure of aerogel limit Phonon heat transfer. On the other hand, the shielding effect due to reflection and refraction by the infinite number of pores can minimize radiative thermal transfer^[22]. However, the contribution of this mechanism increases with temperature according to Rosseland diffusion approximation^[23]:

$$\lambda_{rad} = \frac{16}{3} \frac{\sigma n T^3}{\rho K_a / \rho_s} \quad (5)$$

Where σ is the Stefan-Boltzmann constant, n is the refractive index, T is the absolute temperature, ρ is the apparent density, K_a is the absorption coefficient and ρ_s is the true density of aerogel. While the radiative thermal transfer is minimal in bulk aerogel, in thin films with high infrared transparency, it contributes significantly to the total thermal conductivity^[24].

The solid thermal conductivity (λ_s) is given by^[25]

$$\lambda_s = \lambda_{s,s} \frac{\rho v}{\rho_s v_s} \quad (6)$$

where $\lambda_{s,s}$, ρ , v , ρ_s , and v_s are the thermal conductivity of the silica, bulk density, phonon velocity for silica aerogel, true density, and phonon velocity for silica, respectively.

However, the thermal contribution due to this mechanism is usually smaller than gas diffusion since it depends on density and is consequently suppressed by aerogel's tortuous network and highly porous structure^[21,22]. Lastly, the gas thermal conductivity mechanism in aerogel is expressed by

$$\lambda_g = \frac{k_g^0}{1 + \alpha Kn} \quad (7)$$

where k_g^0 , α , and Kn represent the thermal conductivity of the gas within aerogel, a constant specific to the gas in the pores, and the Knudsen number, respectively. Kn is the ratio of the gas molecule's mean free path to the aerogel's pore size. When Kn is greater than 1, the diffusion of the gas is inhibited. Since the mean free path of an air molecule (~ 70 nm) is larger than the mesoporous (2-50 nm) pore size of aerogel, the air

molecules will interact with the walls of the pores rather than with each other, consequently suppressing thermal conductivity^[26]. However, larger particles or pores than the mean free path of air would contribute to the total thermal conductivity.

During the sol-gel process, the concentration of the reagents was tailored to regulate the network of the aerogel film. The transmittance of all samples is shown in [Supplementary Figure 1](#), [Figure 2A](#) and [Supplementary Figure 2A](#). The A2 sample with the lowest haze of 8.96% exhibited excellent transmittance, exceeding 95% across the visible spectrum. The average transmittance of A2 can reach an astonishing 97.83% [[Table 1](#)]. Pilkington Optifloat™ Clear, commonly used in windows, typically exhibits a visible light transmittance of about 90% at a thickness of 2 mm, which is lower than that of A2 aerogel. This proves that A2 meets the lighting requirement of building windows. Additionally, when Pilkington Optifloat™ Clear is used in multi-pane glazing systems, where multiple glass layers are separated by air or gas to reduce overall thermal conductivity, the total light transmittance decreases as the overall thickness increases^[5]. Further, we analyzed the thermal conductivity of the above samples (A2, M2, U2, D3, and C1) as shown in [Figure 2B](#). The results show that A2 has the lowest thermal conductivity of $0.0149 \text{ W}\cdot\text{m}^{-1}\cdot\text{K}^{-1}$, which proves that this film has the potential for thermal insulation applications. Moreover, its alcogel film also exhibits high transmittance.

The mechanical properties of aerogel film and the ability to retain optical properties after damage are essential in practical applications. The stress (δ)-strain (ϵ) curves for samples A2, M2, U2, C1, and D3 were examined to explore the mechanical properties of aerogel films [[Figure 2C](#)]. The maximum linear elastic regions (a material regains its original size upon removal of stress) correspond approximately to 27%, 18%, 24%, 26%, and 46% for A2, M2, U2, C1, and D3, respectively, reflecting the elastic deformation of the skeleton network. The calculated moduli [[Supplementary Figure 2B](#)] for A2, M2, U2, C1, and D3 were 0.186, 0.174, 0.177, 0.167, and 0.0105 MPa, respectively. After the elastic interval, the network skeleton of the aerogel enters into irreversible compressed deformation. In our experiment, the maximum compressive strain values of the above samples corresponded to 53% (compression strength 0.37 MPa), 47.3%, 51.8%, 54.2%, and 70.1%, respectively. Nevertheless, compared with conventional glass, some aerogel films can maintain higher transmittance after compression. For example, the average transmittance of both A2 and D3 samples in the visible light spectrum exceeds 75%, demonstrating the robustness of the films' transmittance against mechanical deformation [[Figure 2D](#)].

During the formation of the network, controlling polymerization in the sol-gel process according to the pre-designed procedure is quite challenging. Therefore, the network skeleton of aerogel is usually random and can be divided into a uniform network and an uneven network [[Figure 3A](#)]. The narrow pore distribution reflects the uniform network structure, and vice versa for the uneven network structure. The uniform network structure exhibits minimal formation of large particles, leading to an aerogel with lower haze and higher transmittance. At the same time, this network suppresses the formation of large pores ($Kn > 1$), thereby favoring low thermal conductivity. N_2 adsorption-desorption analysis and SEM were used to characterize the pore structure of aerogel samples [[Supplementary Figure 3](#) and [Figure 3B-F](#)]. All samples have a high mesoporous SSA of over $700 \text{ m}^2\cdot\text{g}^{-1}$. Among them, the A2 sample with an average pore size of 12.6 nm has the most uniform network structure, with most pore sizes distributed in the range of 10-40 nm [[Supplementary Figure 3A](#) and [Figure 3B](#)].

The network structure and pore size distribution of M2 and U2 closely resemble that of A2, as shown in [Supplementary Figure 3B and C](#), and [Figure 3C and D](#). However, agglomerated particles contribute to an increase in the pore size distribution by approximately 10 nm. D3 and C1 samples have a wide range of pore

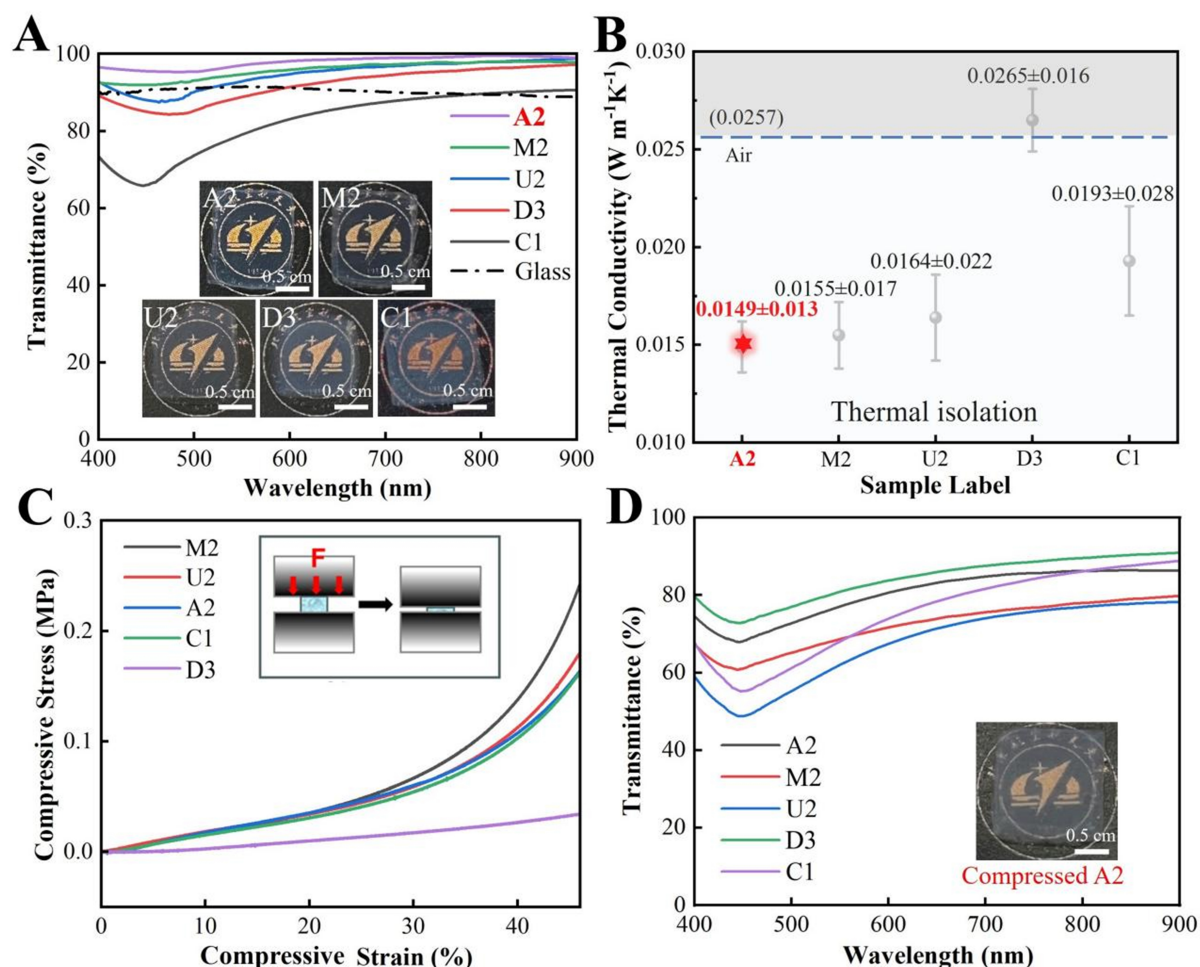


Figure 2. Characterization of aerogel film samples. (A) UV-vis spectra of 3 mm-thick aerogel films and 1 mm glass as a reference. The samples with the highest transmittance in each group are displayed. Inserts of (A) are the optical images of the samples; (B) Thermal conductivity of aerogel films; (C) Compressive stress-strain curves for the aerogel films. Insert of (C) are the compression diagrams; (D) UV-vis spectra for aerogel films after mechanical compression. Insert of (D) is an optical image of A2 after compression. UV-vis: Ultraviolet-visible.

size distribution, presenting the increased small (< 10 nm) and large (> 40 nm) pores, demonstrating an uneven network [Supplementary Figure 3D and E, Figure 3E and F]. The uniform network structure and smaller pore size than the wavelength of air are the reasons for the high transmittance and low thermal conductivity of A2. In contrast, an uneven network leads to decreased transmittance and increased thermal conductivity of D3 and C1.

Notably, the mechanical properties of low-density porous cellular materials are controlled by the structural shape of the network and their solid composition properties [Supplementary Materials]. Under optimized conditions, combined with the ability of supercritical drying to preserve structural integrity, the resulting A2 film demonstrates a uniform network [Figure 3B] with a narrow pore size distribution [Supplementary Figure 3F]. This uniformity allows for even stress distribution throughout the film, thereby enhancing its mechanical properties. In contrast, particle aggregation [Figure 3C-F] and a broad pore size distribution resulted in a non-uniform network where particles are weakly connected through limited contact points and fragile bonds^[27]. These network flaws contributed to progressive mechanical degradation. Furthermore,

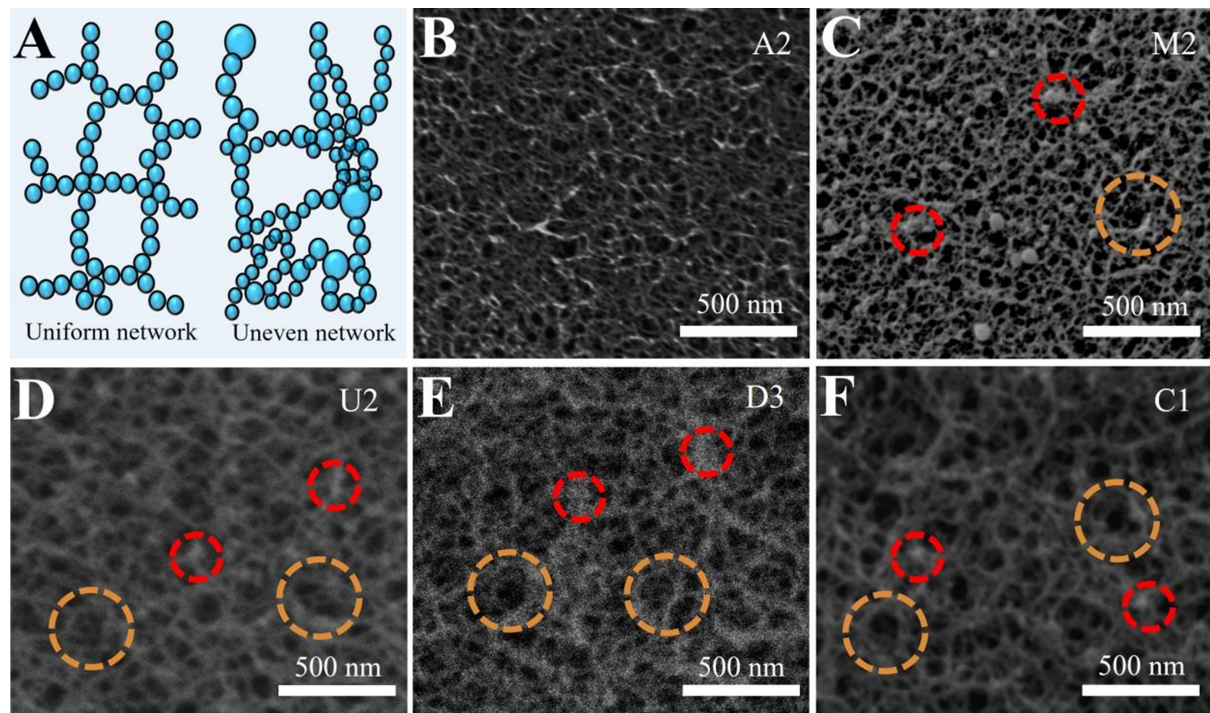


Figure 3. Network structure of aerogel film samples. (A) Diagrams of a uniform network and an uneven network; (B-F) SEM micrographs of silica aerogel films. The red circle represents typical agglomerated particles, and the orange areas represent typically large holes that facilitate gas diffusion. SEM: Scanning electron microscopy.

larger pores acted as stress concentrators, making the skeleton vulnerable to collapse under minimal external stresses, as evidenced by the D3 film. Meanwhile, modifications to the microstructure of aerogel directly influence its optical properties. For example, after compression, the transmittance of all aerogel films decreased, as illustrated in Figure 2D. This was attributed to the densification of the aerogel films following the microstructure collapse. The refractive index (n) of aerogel is fundamentally dependent on density according to the equation $n = 1 + k\rho$, where k and ρ represent a coefficient that varies with light wavelength and the density of silica aerogel, respectively^[21]. Therefore, the increased density led to an increase in refractive index, enhancing light scattering.

Considering transmittance, haze, and thermal conductivity [Supplementary Table 1], A2 is the most suitable aerogel film for windows in this work. Moreover, the thermal conductivity and transmittance of A2 are highly competitive with those of other glazing materials, as shown in Supplementary Table 2. Therefore, application designs for A2 are further carried out. We incorporated an A2 sample as a sandwich between two pieces of glass as “aerogel-glass (AeG)”. The results show that the average transmittance of the AeG (82.3%) in the visible light region is slightly lower than that of ordinary double glass (88.9%) [labeled as “air-glass (AG)”] [Figure 4A]. Under two weeks of continuous 1 Sun irradiation, the A2 film retained consistent transmittance, demonstrating remarkable stability.

In practical applications, glazing materials require stability in a humid environment. As shown in Figure 4B, the infrared absorption spectrum indicates that the A2 aerogel film is mainly composed of silicon-oxygen bonds and contains methyl groups on the surface, which is the origin of hydrophobicity [Figure 4B]^[28]. Additionally, a water drop test confirmed the hydrophobic nature of the A2 aerogel film, where a drop of water applied on the surface beads up [Supplementary Movie 1]. Due to its hydrophobic nature, the A2 film

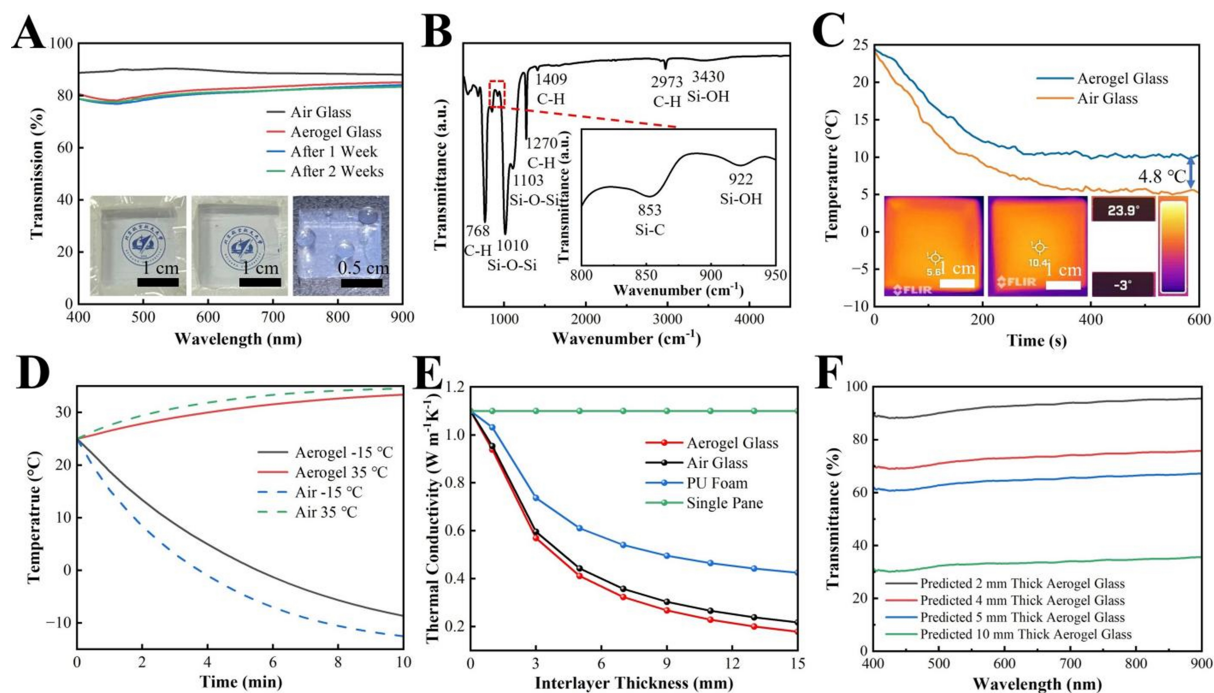


Figure 4. Application analysis of A2 samples as glass interlayers. (A) Comparison of the transmittance of ordinary air-glass and AeG (including transmittance after prolonged irradiation under 1 Sun density); (B) The FTIR spectrum of the A2 sample. Insert of (B) shows the FTIR spectrum of the corresponding wavenumber (800-950 cm⁻¹); (C) Temperature curve over time when air-glass and AeG are placed on ice; (D) Simulated temperature-time graph of an aerogel-filled double-pane window under summer and winter conditions; (E) Thermal conductivity-interlayer thickness graph of simulated thermal conductivity of aerogel-filled double pane glass, air-filled double pane glass, PU-filled double pane glass, and single glass; (F) The calculated transmittance of AeG with different thicknesses of aerogel interlayer. AeG: Aerogel-glass; FTIR: Fourier transform infrared.

is stable in humid air and can withstand collapse when it comes into contact with water. The TG curve in [Supplementary Figure 4](#) shows that A2 aerogel can withstand a temperature of 410 °C before degradation. This temperature is much higher than the practical glazing application scenario in building windows, demonstrating the film's thermal stability.

Further, we compared the thermal insulation properties of AG and AeG [Figure 4C]. In this case, the temperature drop rate of the AeG is significantly lower than that of the AG, and the final temperature of the AeG is about 4.8 °C higher than that of the AG. The above results demonstrate that AeG exhibits excellent transmittance and enhanced thermal shielding properties compared to AG, as well as hydrophobic characteristics and outstanding stability, making it an ideal material for energy-saving windows. We also adopted simulations to verify the thermal insulation properties of the AeG. We set the room temperature at 25 °C, and the ambient temperature of the aerogel at -15 °C (simulating winter) and 35 °C (simulating summer). The results show that the thermal insulation performance of the AeG is superior to that of the AG at the set temperatures [Supplementary Figure 5]. At the same time, the thermal insulation effect of aerogel is more significant under the simulated conditions of -15 °C, demonstrating that the AeG is more suitable for freezing climates [Figure 4D].

We also explored the effect of the thickness of the aerogel interlayer on the thermal conductivity and transmittance, to guide the reasonable choice of the film thickness. The transmittance of AeG at different thicknesses was calculated according to ^[29,30]

$$T = A \times \exp\left(-\frac{Bt}{\lambda^4}\right) \quad (8)$$

where A is the wavelength-independent coefficient representing the surface damages, B describes the wavelength-dependent coefficient from Rayleigh scattering, and t is the thickness of the aerogel film. The results show that the thermal insulation gap between aerogel and common window materials gradually increases with the increase of thickness, starting from the thickness of 3 mm [Figure 4E]. The AeG has the same transmittance as the AG at a thickness of 2 mm and can also maintain a high transmittance before reaching a thickness of 5 mm [Figure 4F].

Real-world integration concerns for insulated glass units (IGU) involve several key issues related to sealing, aging, and condensation. Seal failure can occur due to manufacturing defects or the degradation of seal materials over time. Oxidation caused by oxygen exposure can render sealants brittle. Pressure and temperature fluctuations affect elasticity and accelerate physical deterioration. These failures may lead to the ingress of moisture or the escape of insulating gas, resulting in internal condensation and fogging, decreased thermal insulation, and reduced efficiency. Consequently, proper sealant materials and spacer bars filled with desiccant are advocated to prevent condensation. However, if the seal is compromised, desiccants will saturate, impacting the unit's functionality and longevity. Over an extended period, the aging IGU materials may outgas, releasing volatile gases that degrade the internal surfaces and lead to the formation of fog and condensation. Additionally, condensation within the cavity can occur when the indoor temperature is low or due to cold outdoor weather. This condensation indicates a failure of seal integrity, allowing moisture ingress. Such ingress lowers thermal insulation, promotes the formation of molds, and causes damage to the frame. To minimize condensation, it's essential to use desiccants, improve ventilation, and ensure proper installation of the IGU system. All these concerns need to be addressed simultaneously to realize energy-efficient windows. Hence, the in-lab experiment results should be examined to relate IGU durability to other performance factors^[31].

CONCLUSION

In summary, the silica aerogel film with transmittance of more than 97% and thermal conductivity of less than $0.015 \text{ W}\cdot\text{m}^{-1}\cdot\text{K}^{-1}$ was fabricated by precisely adjusting the concentrations of the reagents (precursor, solvent, gelation agent, phase separation suppressor, and pH conditions) for the first time. This optimized aerogel has a uniform nanonetwork structure with a narrow pore size distribution range of 10-40 nm, effectively suppressing light scattering. In addition, the average pore size of 12.6 nm (well below the mean free path of air, which is 70 nm) efficiently limits the thermal diffusivity of air molecules, which is the main reason for the superior insulation ability of this film. Finally, the results of COMSOL simulations and control experiments collectively demonstrate that this aerogel, with a thickness of 3 mm, can effectively improve the thermal insulation of windows when used as a sandwich. In brief, our work offers optimized processing parameters for fabricating silica aerogel with excellent transmittance and thermal insulation, and the resulting film demonstrates significant potential for use in energy-efficient buildings.

DECLARATIONS

Authors' contributions

Prepared aerogel films, performed most measurements, simulations, and characterization, processed the raw data, and wrote the draft: Momanyi, N. K.; Zhao, P.; Liu, X.

Participated in the partial experimental measurements: Sun, N.; Hu, T.

Participated in the planning of the experimental analysis: Sun, J.

Participated in the design of the experimental scheme and the revision of the manuscript: Liu, L.

Designed the main experimental scheme, guided the experimental implementation, and revised the manuscript: Xie, Y.

Availability of data and materials

The data that support the findings of this study are available from the corresponding author upon reasonable request.

Financial support and sponsorship

This work was supported by the National Natural Science Foundation of China (Nos. 12074024 and 11774018), the Fundamental Research Funds for the Central Universities, and the Academic Excellence Foundation of BUAA for PhD Students. The authors acknowledge the facilities and the scientific and technical assistance of the Analysis & Testing Center, Beihang University. The authors declare no competing financial interest.

Conflicts of interest

All authors declared that there are no conflicts of interest.

Ethical approval and consent to participate

Not applicable.

Consent for publication

Not applicable.

Copyright

© The Author(s) 2025.

REFERENCES

1. Pérez-Iombard, L.; Ortiz, J.; Pout, C. A review on buildings energy consumption information. *Energy. Build.* **2008**, *40*, 394-8. DOI
2. Zhao, P.; Xie, Y.; Hu, S.; et al. Flexible and transparent bagasse aerogels for thermal regulation glazing. *ACS. Sustainable. Chem. Eng.* **2023**, *11*, 9711-20. DOI
3. Smalyukh, I. I. Thermal management by engineering the alignment of nanocellulose. *Adv. Mater.* **2021**, *33*, e2001228. DOI PubMed
4. Abraham, E.; Cherpak, V.; Senyuk, B.; et al. Highly transparent silanized cellulose aerogels for boosting energy efficiency of glazing in buildings. *Nat. Energy.* **2023**, *8*, 381-96. DOI
5. Aguilar-Santana, J. L.; Jarimi, H.; Velasco-Carrasco, M.; Riffat, S. Review on window-glazing technologies and future prospects. *Int. J. Low. Carbon. Technol.* **2020**, *15*, 112-20. DOI
6. Yan, M.; Pan, Y.; Cheng, X.; et al. "Robust-soft" anisotropic nanofibrillated cellulose aerogels with superior mechanical, flame-retardant, and thermal insulating properties. *ACS. Appl. Mater. Interfaces.* **2021**, *13*, 27458-70. DOI PubMed
7. Sun, X.; Sun, H.; Wo, Z.; Su, Y.; Zhang, X. A dual-crosslinked macroporous aerogel with enhanced mechanical durability for efficient solar-driven desalination of seawater and wastewater. *J. Mater. Chem. A.* **2024**, *12*, 29538-49. DOI
8. Wang, C.; Bai, L.; Xu, H.; Qin, S.; Li, Y.; Zhang, G. A review of high-temperature aerogels: composition, mechanisms, and properties. *Gels* **2024**, *10*, 286. DOI PubMed PMC
9. Zhao, S.; Siqueira, G.; Drdova, S.; et al. Additive manufacturing of silica aerogels. *Nature* **2020**, *584*, 387-92. DOI PubMed
10. Cotana, F.; Pisello, A. L.; Moretti, E.; Buratti, C. Multipurpose characterization of glazing systems with silica aerogel: in-field experimental analysis of thermal-energy, lighting and acoustic performance. *Build. Environ.* **2014**, *81*, 92-102. DOI
11. Lian, M.; Ding, W.; Liu, S.; et al. Highly porous yet transparent mechanically flexible aerogels realizing solar-thermal regulatory cooling. *Nanomicro. Lett.* **2024**, *16*, 131. DOI PubMed PMC
12. Illera, D.; Mesa, J.; Gomez, H.; Maury, H. Cellulose aerogels for thermal insulation in buildings: trends and challenges. *Coatings* **2018**, *8*, 345. DOI
13. Long, L. Y.; Weng, Y. X.; Wang, Y. Z. Cellulose aerogels: synthesis, applications, and prospects. *Polymers* **2018**, *10*, 623. DOI PubMed PMC
14. Wang, X.; Yang, X.; Wu, Z.; et al. Enhanced mechanical stability and hydrophobicity of cellulose aerogels via quantitative doping of nano-lignin. *Polymers* **2023**, *15*, 1316. DOI PubMed PMC
15. Liu, J.; Liu, J.; Shi, F.; et al. A facile pore size controlling strategy to construct rigid/flexible silica aerogels for super heat insulation

- and VOCs adsorption. *Chem. Eng. J.* **2022**, *450*, 138196. DOI
16. Hayase, G.; Kanamori, K.; Nakanishi, K. Structure and properties of polymethylsilsesquioxane aerogels synthesized with surfactant *n*-hexadecyltrimethylammonium chloride. *Micropor. Mesopor. Mat.* **2012**, *158*, 247-52. DOI
 17. Gupta, P.; Sathwane, M.; Chhajed, M.; et al. Surfactant assisted in situ synthesis of nanofibrillated cellulose/polymethylsilsesquioxane aerogel for tuning its thermal performance. *Macromol. Rapid. Commun.* **2023**, *44*, 2200628. DOI
 18. Payanda Konuk, O.; Alsuhile, A. A. A. M.; Yousefzadeh, H.; et al. The effect of synthesis conditions and process parameters on aerogel properties. *Front. Chem.* **2023**, *11*, 1294520. DOI PubMed PMC
 19. Smith, D. S.; Alzina, A.; Bourret, J.; et al. Thermal conductivity of porous materials. *J. Mater. Res.* **2013**, *28*, 2260-72. DOI
 20. Harvey, A.; Backes, C.; Boland, J. B.; et al. Non-resonant light scattering in dispersions of 2D nanosheets. *Nat. Commun.* **2018**, *9*, 4553. DOI PubMed PMC
 21. Wang, J.; Petit, D.; Ren, S. Transparent thermal insulation silica aerogels. *Nanoscale. Adv.* **2020**, *2*, 5504-15. DOI PubMed PMC
 22. Li, C.; Chen, Z.; Dong, W.; et al. A review of silicon-based aerogel thermal insulation materials: performance optimization through composition and microstructure. *J. Non. Cryst. Solids.* **2021**, *553*, 120517. DOI
 23. Fu, Z.; Corker, J.; Papathanasiou, T.; et al. Critical review on the thermal conductivity modelling of silica aerogel composites. *J. Build. Eng.* **2022**, *57*, 104814. DOI
 24. Michael, M.; Favoino, F.; Jin, Q.; Luna-Navarro, A.; Overend, M. A systematic review and classification of glazing technologies for building façades. *Energies* **2023**, *16*, 5357. DOI
 25. Lee, O.; Lee, K.; Jin Yim, T.; Young Kim, S.; Yoo, K. Determination of mesopore size of aerogels from thermal conductivity measurements. *J. Non. Cryst. Solids.* **2002**, *298*, 287-92. DOI
 26. Roiban, L.; Foray, G.; Rong, Q.; et al. Advanced three dimensional characterization of silica-based ultraporous materials. *RSC. Adv.* **2016**, *6*, 10625-32. DOI
 27. Zhan, W.; Chen, L.; Kong, Q.; et al. The synthesis and polymer-reinforced mechanical properties of SiO₂ aerogels: a review. *Molecules* **2023**, *28*, 5534. DOI PubMed PMC
 28. Zhao, P.; Peng, J.; Momanyi, N. K.; et al. Black aerogel based on short-time high-flux He ion implantation. *Adv. Funct. Mater.* **2025**, *35*, 2408995. DOI
 29. Hunt, A. J. Light scattering for aerogel characterization. *J. Non. Cryst. Solids.* **1998**, *225*, 303-6. DOI
 30. Zhao, L.; Yang, S.; Bhatia, B.; Strobach, E.; Wang, E. N. Modeling silica aerogel optical performance by determining its radiative properties. *AIP. Adv.* **2016**, *6*, 025123. DOI
 31. Likins-White, M.; Tenent, R. C.; Zhai, Z. Degradation of insulating glass units: thermal performance, measurements and energy impacts. *Buildings* **2023**, *13*, 551. DOI